Progress In Electromagnetics Research C, Vol. 173, 190–197, 2026

PIER C

(Received 20 July 2026, Accepted 27 August 2026, Scheduled 8 September 2026)

Krylov Subspace Acceleration by Adaptive Cross Approximation for Improved CBFM Electromagnetic Scattering Computation

Xiaofei Ma[1], Zhonggen Wang[1], Wenyan Nie[2,*], and Han Lin[1]

[1]School of Electrical and Information Engineering, Anhui University of Science and Technology, Huainan 232001, China
[2]School of Mechanical and Electrical Engineering, Huainan Normal University, Huainan 232001, China

ABSTRACT: To resolve the trade-off between numerical accuracy and computational efficiency when integrating the adaptive cross approximation (ACA) into the characteristic basis function method (CBFM), this study proposes a hybrid optimization framework incorporating Krylov subspaces. This framework first employs CBFM to partition scattering targets into multiple subdomains and realize the dimension reduction of the impedance matrix. The ACA algorithm is then adopted to perform low-rank compression on far-field coupling submatrices. Therefore, the GMRES algorithm was introduced to implement iterative optimization. The framework uses the approximate solution from the CBFM as the initial iterative guess and leverages the ACA to accelerate constructing Krylov subspaces to reduce the iterative computational overhead. Numerical results of two sets of test cases demonstrate that, compared with the traditional coupled CBFM-ACA solver, the proposed method can significantly improve numerical accuracy while maintaining favorable computational efficiency.

1. INTRODUCTION

Numerical analysis of electromagnetic scattering has vital applications in radar detection, target recognition, stealth design, wireless communications, and other fields. Radar cross section (RCS) [1] is a standard parameter for characterizing target scattering properties, and its accurate evaluation generally relies on numerical algorithms. The method of moments (MoM) [2, 3] is a classical full-wave solver for electromagnetic scattering problems. It discretizes integral equations to extract induced surface currents on scatterers, featuring high computational accuracy and broad applicability. Nevertheless, for electrically large or geometrically intricate targets, the impedance matrix yielded by the MoM discretization is dense, which imposes heavy computational burdens in matrix assembly, storage, and solution procedures. To mitigate the computational complexity, a series of acceleration techniques have been developed for scattering analysis, including the fast multipole method (FMM) [4], multilevel fast multipole algorithm (MLFMA) [5], adaptive cross approximation (ACA) [6, 7], and domain decomposition method (DDM) [8]. These approaches deliver promising performance gains in matrix filling, compressed storage, and iterative solutions.

The characteristic basis function method (CBFM) [9, 10] is a common technique for reducing matrix dimensions. This method generally partitions the scattering target into several subdomains, constructs characteristic basis functions (CBFs) [11–13] within each subdomain to represent local current distributions, and substitutes these CBFs for numerous Rao-Wilton-Glisson (RWG) [14] basis functions in the global solution procedure to reduce the number of unknowns in the original matrix equation. In recent years, research on CBFM has mainly focused on constructing characteristic basis functions, subdomain partitioning, overlapping-region processing, fusion schemes of characteristic basis functions, compression of reduced matrices, and iterative solution algorithms [15, 16]. Some studies have introduced the eigenmode concept into the generation of CBFs to strengthen their capability of characterizing local currents [17]; other studies have combined CBFM with the ACA, preconditioning techniques, or domain decomposition strategies to lower the computational overhead for constructing inter-subdomain coupling matrices and improve overall solution efficiency [18]. Ref. [19] proposed fused improved characteristic basis functions (IPCBFs) constructed by combining primary characteristic basis functions (PCBFs) and secondary characteristic basis functions (SCBFs) to boost computational efficiency. Meanwhile, within the CBFM framework, there exists an inherent trade-off between the number of selected characteristic basis functions and the accuracy of the final solution: if fewer CBFs are adopted, the dimension of the reduced matrix shrinks, and the computational time consumed in the matrix construction stage can be remarkably reduced. Nevertheless, an insufficient number of basis functions degrades CBFM's ability to model full-domain electromagnetic scattering. In contrast, increasing the number of CBFs drastically increases the time cost for constructing the reduced matrix and solving current expansion coefficients.

* Corresponding author: Wenyan Nie (wynie5240@163.com).

Accordingly, an improved strategy with dynamic balance is urgently required and can effectively elevate numerical accuracy while drastically reducing computational overhead and delivering an efficient, accuracy-guaranteed solver for electromagnetic scattering analysis of complex electrically large targets. Therefore, achieving a favorable balance between numerical accuracy and solution efficiency remains an open issue that requires further investigation when applying CBFM to RCS calculation of complex targets.

To address these challenges, this study incorporates the Generalized Minimal Residual(GMRES) algorithm into the CBFM's dimension-reduction framework. The proposed framework first captures the inherent characteristics of the solution via preliminary CBFM computation, then leverages ACA to accelerate Krylov subspace generation [20, 21], and precisely controls the solution accuracy by setting a GMRES convergence threshold. This method adaptively tunes the CBFM's accuracy level, effectively alleviating the fundamental accuracy-efficiency trade-off. The core objective is to increase numerical accuracy for large total number of variables to be solved in the matrix equation engineering problems prone to accuracy degradation, while fully exploiting the inherent merits of CBFM.

2. THEORY

The theoretical section consists of three core components. First, it introduces the CBFM calculation framework and elaborates on its key computational procedures, including calculating characteristic basis functions, constructing reduced matrices, and solving current coefficients. Second, it conducts an in-depth analysis of the principle of iteration acceleration based on the ACA and the theoretical innovations proposed for the Krylov subspace construction stage. Finally, it presents the implementation procedure of the GMRES algorithm, which is adopted to further improve the CBFM's performance.

2.1. CBFM Framework

In computational electromagnetics, triangular meshes are commonly used to discretize the surfaces of conductors, dielectrics, and other targets to solve electromagnetic scattering problems. Each interior edge shared by two adjacent triangular elements corresponds to a unique RWG vector-based function. Using RWG vector basis functions, the MoM converts the surface integral equation of three-dimensional targets into the matrix equation presented below:

$$\mathbf{ZI} = \mathbf{V} \tag{1}$$

where $\mathbf{Z}$ denotes an $N \times N$ dimensional full-rank impedance matrix, and N represents the number of RWG basis functions. $\mathbf{I}$ and $\mathbf{V}$ denote the $N \times 1$ dimensional unknown induced current and incident excitation vector, respectively. The elements of $\mathbf{Z}$ and $\mathbf{V}$ are expressed by the following equations:

$$\begin{aligned} Z_{mn} &= j\omega\mu_0 \iint_{S_m} \iint_{S_n} G \cdot \Big(f_m(r) \cdot f_n(r') \\ &\quad - j\frac{1}{\omega^2 \mu_0 \varepsilon_0} \cdot \nabla \cdot f_m(r) \cdot \nabla' \cdot f_n(r') \Big) dS' dS \end{aligned} \tag{2}$$

$$V_m = -\iint_{S_m} f_m(r) \cdot \mathbf{E}^{inc}(r)\, dS \tag{3}$$

where ω, μ_0, and ε_0 denote the angular frequency, vacuum permeability, and permittivity, respectively; G represents the Green's function; $f_m(r)(f_n(r'))$ denotes the $n(m)$-th RWG basis function; and $\mathbf{E}^{inc}(r)$ represents the incident electric field. In CBFM, subdomain decomposition is first required to divide the target into M subdomains. Because this partitioning alters the target geometry and causes discontinuities in the surface current distribution, each subdomain must be extended to address this issue, leading to the transformation:

$$\begin{bmatrix} \mathbf{Z}_{11} & \mathbf{Z}_{12} & \mathbf{Z}_{13} & \cdots & \mathbf{Z}_{1M} \\ \mathbf{Z}_{21} & \mathbf{Z}_{22} & \mathbf{Z}_{23} & \cdots & \mathbf{Z}_{2M} \\ \vdots & \vdots & \vdots & \cdots & \vdots \\ \mathbf{Z}_{M1} & \mathbf{Z}_{M2} & \mathbf{Z}_{M3} & \cdots & \mathbf{Z}_{MM} \end{bmatrix} \begin{bmatrix} \mathbf{J}_1 \\ \mathbf{J}_2 \\ \vdots \\ \mathbf{J}_M \end{bmatrix} = \begin{bmatrix} \mathbf{E}_1 \\ \mathbf{E}_2 \\ \vdots \\ \mathbf{E}_M \end{bmatrix} \tag{4}$$

where $\mathbf{Z}_{mm}$ denotes the self-impedance matrix of the m-th subdomain with dimension $N_m \times N_m$, and $\mathbf{Z}_{mn}$ represents the mutual impedance matrix with dimension $N_m \times N_n$. N_m and N_n denote the number of unknowns in subdomain m and subdomain n.

The common method for generating CBFs is as follows: Assume that N_θ and N_ϕ are the numbers of incident plane wave excitations in θ and ϕ directions, respectively. Considering two polarizations, a total of $N_{IPW} = 2N_\theta N_\phi$ incident plane wave excitations are required. CBFs for each subdomain can be obtained by the following equation.

$$\mathbf{Z}_{ii}^e \cdot \mathbf{J}_{ii}^e = \mathbf{V}_{ii}^{N_{IPW}} \tag{5}$$

where $\mathbf{Z}_{ii}^e$ denotes the self-impedance matrix of the i-th extended subdomain with dimension $N_i^e \times N_i^e$; N_i^e denotes the dimension of the i-th subdomain after extension; $\mathbf{V}_{ii}^{N_{IPW}}$ is the excitation matrix of size $N_i^e \times N_{IPW}$; $\mathbf{J}_{ii}^e$ represents the current coefficient matrix for the i-th subdomain, whose dimension is $N_i^e \times N_{IPW}$.

The redundant information in $\mathbf{J}_{ii}^e$ is eliminated using truncated singular value decomposition (SVD). Specifically, a threshold δ is set to discard normalized eigenvalues whose magnitudes are smaller than δ. $\mathbf{J}_i$ denotes the subdomain CBFs after SVD screening. Accordingly, the overall basis function set $\mathbf{J}_{cbf}$ can be expressed as

$$\mathbf{J}_{cbf} = \begin{bmatrix} \mathbf{J}_1 & 0 & \cdots & 0 \\ 0 & \mathbf{J}_2 & \cdots & 0 \\ \vdots & \vdots & \ddots & \vdots \\ 0 & 0 & \cdots & \mathbf{J}_M \end{bmatrix} \tag{6}$$

Then, construct reduced matrices $\mathbf{Z}_{cbf}$ and $\mathbf{V}_{cbf}$:

$$\mathbf{Z}_{cbf} = \mathbf{J}_{cbf}^H \mathbf{Z} \mathbf{J}_{cbf} \tag{7}$$

$$\mathbf{V}_{cbf} = \mathbf{J}_{cbf}^H \mathbf{V} \tag{8}$$

where the current coefficients are denoted as α, and the lower-upper (LU) decomposition is adopted to accelerate the computation of the reduced-dimensional matrix:

$$\mathbf{Z}_{cbf}\alpha = \mathbf{V}_{cbf} \tag{9}$$

The relationship between the original current $\mathbf{I}_0$ and the current coefficient α is given by

$$\mathbf{I}_0 = \mathbf{J}_{cbf}\alpha \tag{10}$$

2.2. Proposed Method

When constructing the impedance matrix via the CBFM, the global matrix is partitioned into multiple sub-block matrices, which are further classified into near-field and far-field groups according to a specified threshold parameter. The electromagnetic coupling strength between different subdomains of the target decays with increasing distance, making far-field coupling matrices inherently low rank. In contrast, near-field regions exhibit strong coupling and possess high matrix ranks; therefore, they are computed exactly to guarantee the solution accuracy of strongly coupled regions. The decomposition formula for the far-field matrix $\mathbf{Z}_{ij}$ is as follows:

$$\mathbf{Z}_{ij}^{N_i \times N_j} \approx \mathbf{Z}_u^{N_i \times r_{ij}} \mathbf{Z}_v^{r_{ij} \times N_j} \tag{11}$$

Via ACA low-rank decomposition, a far-field sub-block can approximately factorize the original dense matrix into two low-rank submatrices $\mathbf{Z}_u(N_i \times r_{ij})$ and $\mathbf{Z}_v(r_{ij} \times N_j)$. Here, r_{ij} denotes the truncated effective rank of ACA, which is substantially smaller than the row and column dimensions N_i and N_j of the original matrix, respectively. Figure 1 shows a schematic diagram of far-field impedance matrix decomposition with the ACA algorithm.

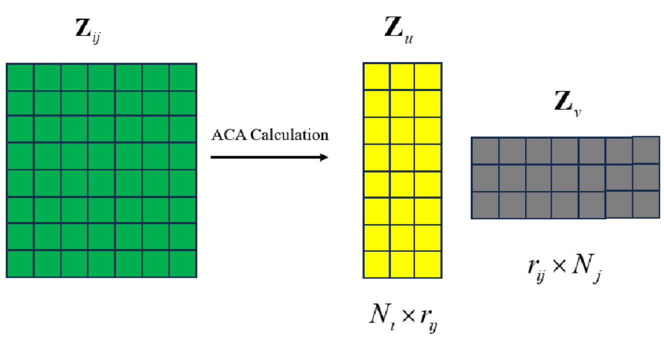

FIGURE 1. Flowchart of far-field impedance matrix decomposition with the ACA algorithm.

To improve the computational efficiency of the ACA algorithm, a reasonable classification of far-field and near-field interactions is required [22]. Let d denote the distance between subdomains i and subdomain j, and c represent the size of each subdomain. If the distance d satisfies $d > 0.05\lambda$ (where λ is the wavelength of the incident excitation) and $d > pc$ (p is a preset parameter), the corresponding submatrix $\mathbf{Z}_{ij}$ is compressed by the ACA algorithm.

To address the trade-off between numerical accuracy and computational efficiency induced by characteristic basis functions, this study proposes a novel scheme that incorporates the GMRES algorithm for iterative correction. The ACA was adopted to streamline the computing pipeline, reduce the overall computational load, and accelerate the construction of Krylov orthogonal bases during the Arnoldi iterations. In practical implementation, GMRES is performed on the impedance matrix filled and compressed by ACA, with the preliminary solution from the CBFM as the initial guess. The advantages of the proposed method are summarized as follows: Even if the raw solution yielded by the CBFM suffers from insufficient precision, the proposed approach can always converge to an arbitrarily prescribed error tolerance. When the CBFM solution already meets the accuracy requirement, the final iterative procedure can be skipped to directly acquire the scattering solution. In other words, this method enables flexible precision regulation, and favorable numerical accuracy can be achieved within only a small number of iterations. To improve the computational efficiency of Krylov subspace computation, all original full-size far-field submatrices are replaced by low-rank counterparts compressed via ACA, and the execution order of matrix-vector multiplications is further optimized to reduce redundant floating-point operations.

ACA-accelerated matrix-vector multiplication is used to generate the standard Krylov subspace method. Figure 2 presents its complete schematic diagram. ACA-accelerated matrix-vector multiplication is used to generate the standard Krylov subspace method. For a given subdomain i, the corresponding calculation formula can be transformed as follows:

$$\mathbf{Z}_{ij} \cdot v_i \approx \mathbf{Z}_u \cdot (\mathbf{Z}_v \cdot v_i) \tag{12}$$

Algorithm 1 elaborates specific steps for generating the Krylov subspace via the Arnoldi iteration to facilitate the understanding of the implementation mechanism of the GMRES algorithm. As a core component of GMRES, the Arnoldi iteration constructs an orthogonal basis that spans the entire Krylov subspace.

From a logical perspective, embedding the GMRES algorithm into the CBFM framework offers remarkable advantages. First, the proposed scheme can seamlessly interface with the construction and solution architecture of the reduced matrix in the conventional CBFM, and only the GMRES iterative module needs to be invoked to update the original solution vector. Second, the CBFM's inherent core merits, including acceleration via order reduction and reducing system matrix dimension and number of unknowns, are fully retained. Meanwhile, GMRES features fast convergence and native compatibility with asymmetric dense impedance matrices. It can be iterated until a prescribed residual threshold is reached to flexibly regulate the solution accuracy, further mitigating the accuracy degradation caused by the order-reduction operation.

3. COMPLEXITY ANALYSIS

To quantitatively evaluate the performance merits of the hybrid algorithm proposed in this section when tackling complex electromagnetic targets, we conducted a computational complexity analysis of the CBFM-ACA-GMRES hybrid method developed in this study. Let the total number of unknowns of the target be N, and the target be partitioned into M subdomains, with the average number of unknowns per subdomain denoted as $N_i \approx N/M$.

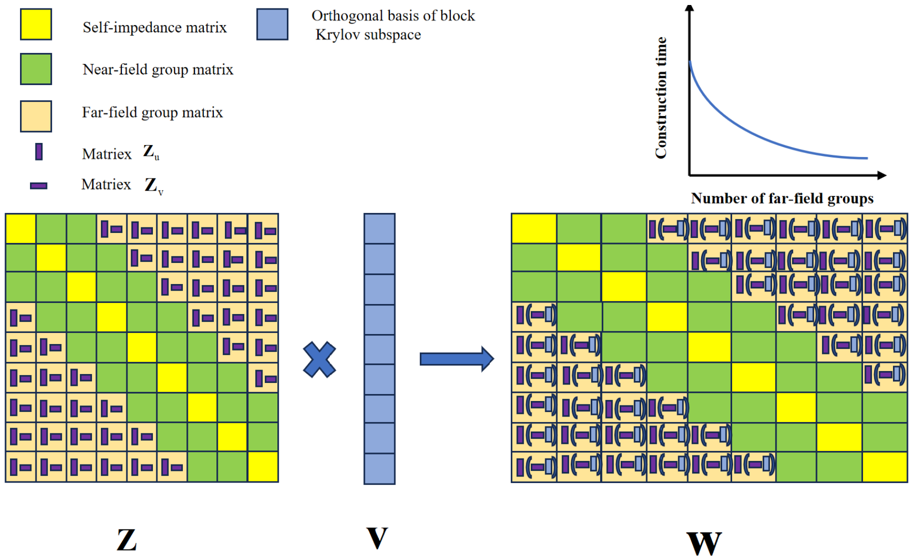

FIGURE 2. Accelerated construction of Krylov subspace basis functions via ACA.

Algorithm 1: Accelerated Arnoldi Iteration for Krylov Subspace Generation Based on ACA

Input: Coefficient matrix $\mathbf{Z} = \mathbf{Z}_{near} + \mathbf{Z}_{far}$, ACA factorization $\mathbf{Z}_{far} \approx \mathbf{Z}_u \bullet \mathbf{Z}_v$, Initial vector $\mathbf{V}$,

Initial solution $\mathbf{I}_0$, iterations m

Output: Orthogonal basis $\mathbf{V}_{m+1} = [\mathbf{v}_1, \mathbf{v}_2, \ldots, \mathbf{v}_{m+1}]$

Set $\mathbf{r} = \mathbf{E} - \mathbf{Z} \bullet \mathbf{I}_0$, $\mathbf{v}_1 = \mathbf{r} / \|\mathbf{r}\|$
  for $i = 1, 2, 3, \cdots, m$ **do**
    Solve $\mathbf{w}_i \approx \mathbf{Z}_{near}\mathbf{v}_i + \mathbf{Z}_u\left(\mathbf{Z}_v \bullet \mathbf{v}_i\right)$
    for $j = 1, 2, 3, \cdots, i$ **do**
      Solve $h_{i,j} = (\mathbf{w}_i, \mathbf{v}_j)$, $\mathbf{w}_i = \mathbf{w}_i - h_{i,j} \bullet \mathbf{v}_j$
    end for
    Solve $h_{i+1,i} = \|\mathbf{w}_i\|_2$
    if $h_{i+1,i} = 0$
      break
    end if
    Set $\mathbf{v}_{i+1} = \mathbf{w}_i / h_{i+1,i}$
  end for
Generate an orthogonal basis of the subspace $\mathbf{V}_{m+1} = \left[\mathbf{v}_1, \mathbf{v}_2, \cdots, \mathbf{v}_{m+1}\right]$

3.1. Complexity of Impedance Matrix Filling

The matrix-filling complexity of conventional methods is $O(N^2)$. When low-rank compression is performed using the ACA algorithm, the near-field blocks near the diagonal are fully assembled. However, for far-field mutual impedance subblocks that account for a large proportion of the matrix, the ACA algorithm avoids computing all matrix entries. For a far-field block matrix of size $N_i \times N_j$, we only extract the effective rank by setting a threshold. Consequently, the filling complexity is drastically reduced from the original $O(N_i \times N_j)$ to $O(r_{ij}(N_i + N_j))$, where $r_{ij} \ll (N_i, N_j)$. Due to the low-rank property of far-field interactions, this procedure substantially reduces the computational and memory overhead required to assemble the entire impedance matrix.

3.2. Complexity of Krylov Subspace Iteration

As the core component of the GMRES algorithm, the Arnoldi iteration constructs orthogonal basis vectors to span the Krylov subspace. The computational cost of the iterative process directly governs the GMRES' overall solution efficiency. We now analyze the computational complexity associated with Krylov subspace construction. The primary computational burden of this procedure stems from repeatedly executing matrix-vector multiplications, the most time-consuming operation in electrically large electromagnetic scattering simulations. Combined with the ACA low-rank compression scheme introduced earlier, far-field coupling matrices no longer participate in computations in their original dense form, effectively reducing the arithmetic cost of each matrix-vector multiplication.

The computational complexity of the Arnoldi procedure arises mainly from matrix-vector multiplication. One matrix-vector multiplication is required in each iteration step, with a single-step complexity of $O(N^2)$. If the total number of iteration steps is denoted as m, the overall computational complexity is $O(mN^2)$. Nevertheless, when matrix-vector multiplication is implemented in the compressed format via ACA, the complexity of a single operation for the far-field submatrix $\mathbf{Z}_{ij}$ is reduced from $O(N_i \cdot N_j)$ to $O(r_{ij}(N_i + N_j))$. This scheme can effectively reduce the construction time of Krylov subspaces, and the global computational complexity is further optimized to the growth order of $O(mN \log N)$.

3.3. Complexity of Solving the Global Equation

The conventional MoM adopts direct LU decomposition to solve the global impedance matrix equation, which has computational complexity $O(N^3)$. In the hybrid method proposed in this study, the target geometry is partitioned into multiple subdomains. SVD is employed to extract CBFs from each subdomain, which efficiently projects the original large-scale MoM impedance matrix into a low-dimensional space spanned by characteristic basis vectors. Only a small number of valid CBF modes are retained for each subdomain; these modes can capture the inherent features of the induced currents and reconstruct the original current distribution. The GMRES algorithm was then used to conduct sufficient iterations to obtain an accurate current solution. Accordingly, the total global degrees of freedom for solving are drastically reduced from N, the total number of original fine-mesh RWG unknowns, to $K (K \ll N)$, the total count of characteristic basis functions, which yields a reduced impedance matrix with greatly diminished dimensions.

In summary, the hybrid scheme proposed in this study achieves simultaneous complexity reduction across the full computational pipeline, including matrix assembly, subdomain basis extraction, and linear system solving. Theoretical analysis verifies that the proposed method delivers excellent computational efficiency when addressing electrically large targets with intricate electromagnetic couplings.

4. NUMERICAL RESULTS

To verify the validity of the proposed method, in this section, we present several numerical examples to demonstrate the performance of the GMRES algorithm. The root mean square error (RMSE) of the bistatic RCS was adopted as the accuracy metric, which is defined as

$$\text{RMSE} = \sqrt{\frac{1}{N_a}\sum_{i=1}^{N_a}\left(\sigma_{cal} - \sigma_{MoM}\right)^2} \tag{13}$$

where N_a denotes the total number of samples, and σ_{cal} and σ_{MoM} represent the simulated results of the proposed method and reference MoM, respectively.

4.1. Perfect Electrical Conductor Cube

To verify the validity of the proposed method, we performed numerical simulations on a perfect electric conductor (PEC) cube with a side length of 1.1 m. The cube was illuminated by a plane wave with a central frequency of 700 MHz and a polarization angle of 90°. The target surface was discretized using RWG basis functions, generating 13128 triangular facets and 19692 unknowns, each block expanded to 0.15 wavelengths, resulting in 24567 unknowns. In the analysis of this work, the stopping criterion of the GMRES algorithm, namely the residual norm δ_G, was set to 1E-2, and the maximum number of iterations was set to 50.

To quantitatively study the influence of the SVD threshold on the number of retained basis functions in each block, Figure 3 shows adaptive truncation results for eight blocks under different threshold levels. Each color corresponds to a specific SVD threshold value. As the SVD threshold increases, low-energy modes that contribute less to the local subspace are discarded; thus, the number of retained basis functions in each block decreases accordingly. A higher threshold retains more basis functions, and this effect is particularly evident in regions with relatively simple geometric structures.

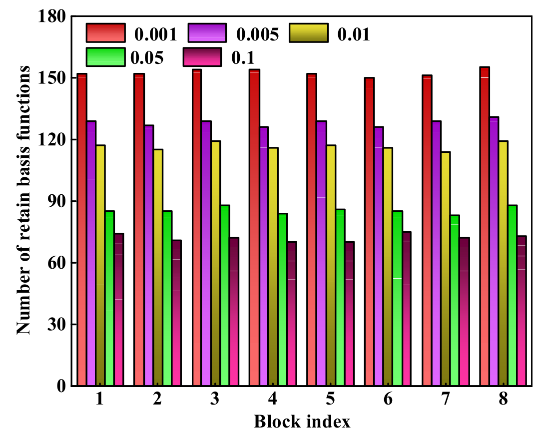

FIGURE 3. The influence of SVD threshold on the retention ratio of spherical basis functions.

First, to investigate the effects of different SVD thresholds δ on solving time and RMSE, Figure 4 shows the solving time and RMSE of the two distinct extraction methods under various truncation thresholds. The solving time covers the construction of the characteristic basis functions and the current

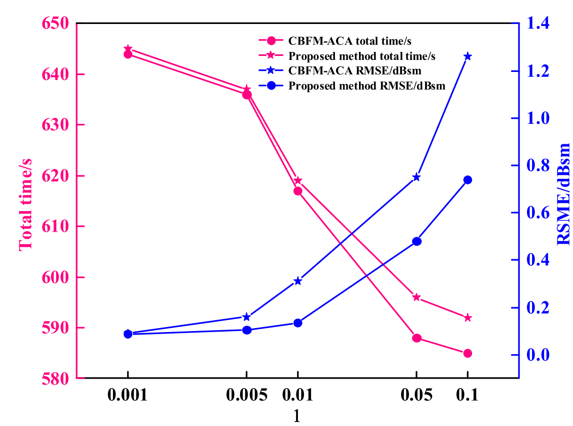

FIGURE 4. Influence of SVD threshold on solving time and RMSE of PEC cube.

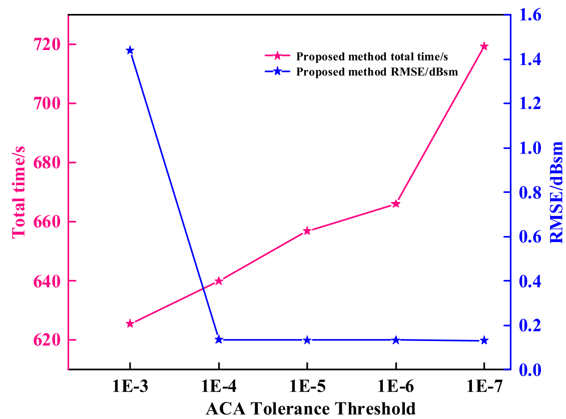

FIGURE 5. Analysis of the effects of ACA truncation threshold on solving time and RMSE.

recovery procedure. When the SVD truncation threshold is set excessively wide, the CBFM initial guess contains considerable errors. Under such circumstances, sufficient convergence cannot be achieved within the predefined maximum number of iterations. The errors originating from the initial guess cannot be completely eliminated and will persist in the final solution. A wider threshold accelerates the construction of CBFM initial guess, and the resulting initial error leads to an increase in iteration steps. A narrower threshold provides a more accurate initial guess with fewer iteration steps, but substantially raises the preprocessing cost for characteristic basis construction. Since the overall computational efficiency is jointly determined by these two factors, a moderate threshold should be selected. As illustrated in Figure 4, combined with ACA, the two methods yield comparable computational times; however, the proposed method consistently produces lower RMSE values than the conventional CBFM-ACA scheme, which demonstrates superior numerical accuracy. This advantage becomes more pronounced when δ exceeds 1E-2.

Figure 5 further analyzes the influence of the ACA truncation threshold on the overall computational performance. In this part, we set the far-field grouping parameter p to 1.4, which yields a total of 32 far-field matrices. Excluding the self-impedance matrix, these far-field matrices account for 57% of the full matrix. As shown in the figure, the model's RMSE output continuously decreases and gradually converges as the threshold becomes tighter. The ultimate convergence is bounded by the inherent error floor of the CBFM framework, and the error reaches its lower limit when the threshold is set to 1E-4. Meanwhile, the solution time shows a monotonic trend, rising persistently with reducing threshold. In summary, the optimal ACA truncation threshold is selected as 1E-4, which achieves a favorable trade-off between computational cost and prescribed precision requirements.

To further validate the accuracy of the proposed method, Figure 6 compares surface current results calculated using this scheme and the MoM. All current data in the figure were acquired via uniform sampling, consisting of 19692 common edge current unknowns. The SVD truncation threshold is set to 1E-2. The number of CBFs was reduced to 933 after the final screening. As shown in Figures 6(a) and 6(b), which correspond to the real and imaginary parts, respectively, the current values obtained using the proposed method are in excellent agreement with those obtained using the MoM. Furthermore, Figure 7 presents the RCS results computed by the CBFM-ACA and the proposed method under the above-mentioned conditions. The horizontally polarized RCS curves of the cube computed using the proposed method perfectly matched the MoM reference data.

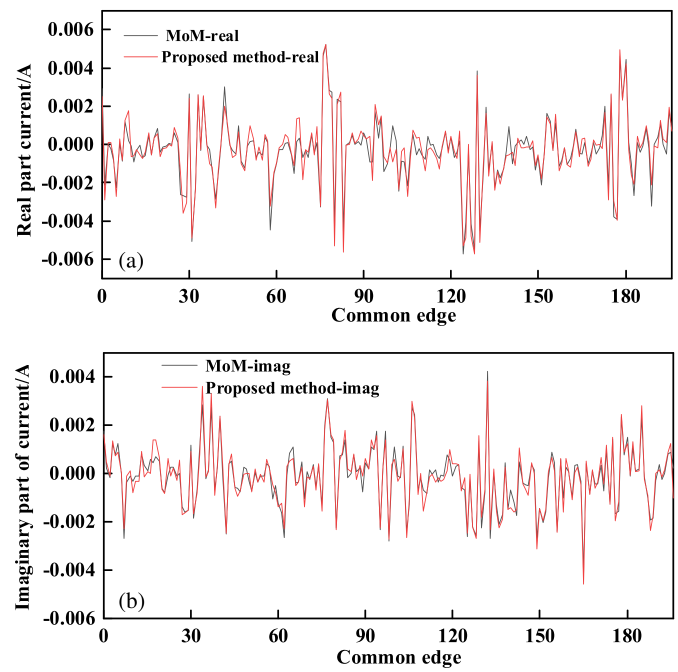

FIGURE 6. Common edge currents. (a) Current real part. (b) Current imaginary part.

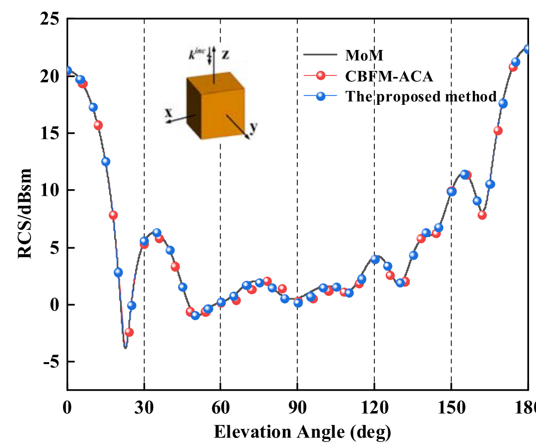

FIGURE 7. Bistatic RCS of PEC cube at 700 MHz.

4.2. Perfect Electrical Conductor Cylinder

To further verify the superiority of the proposed method, a bistatic RCS simulation analysis was performed on a PEC cylindrical model with a base radius of 0.8 m and a height of 2 m. The frequency of the incident electromagnetic wave was set to 800 MHz, and the observed scattering angle range was defined as $(\theta, \phi) = (0°, -180°, 0°)$. The target surface was

TABLE 1. Comparison of the proposed method with traditional methods.

Model	Method	unknowns	Basis function construction (s)	Solving (s)	Total time (s)	RMSE (dBsm)
Cube	CBFM-ACA	19692	528	87	615	0.312
	Proposed method		528	90	618	0.136
Cylinder	CBFM-ACA	51447	8136	2042	10178	1.03
	Proposed method		8136	2758	10894	0.52
Almond	CBFM-ACA	33072	2674	618	3272	0.5
	Proposed method		2664	662	3326	0.287

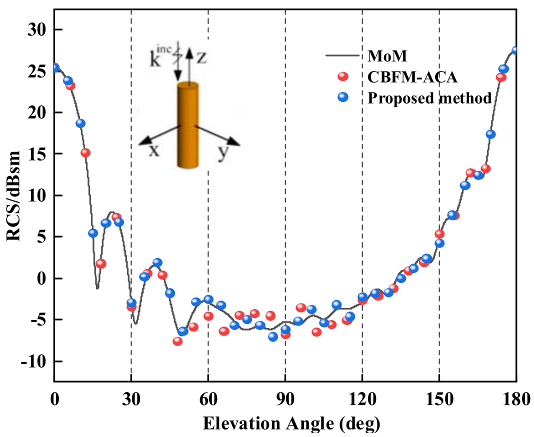

FIGURE 8. Bistatic statistical RCS of a PEC cylinder at 800 MHz.

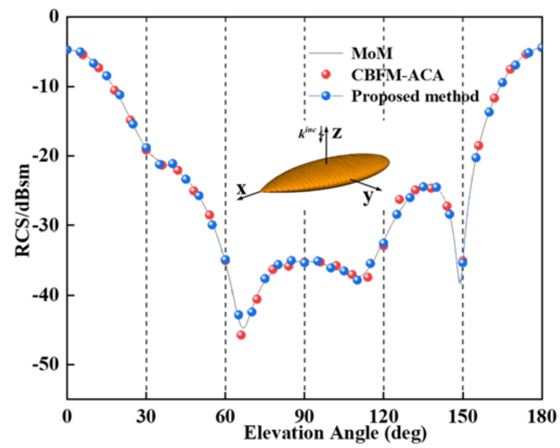

FIGURE 9. Bistatic RCS of the almond in horizontal polarization.

meshed into 34298 triangular elements, resulting in a total of 51447 unknowns. The target's geometric domain was partitioned into eight subdomains, from which 1753 CBFs were constructed. Furthermore, each subdomain was expanded omnidirectionally by a distance of 0.15 wavelengths, and the number of unknowns after expansion increased to 59724. The ACA truncation threshold is uniformly set to 1E-4, and the SVD threshold is set to 1E-2. Figure 8 presents RCS curves obtained using the three approaches. The proposed method achieves excellent agreement with the MoM and has high computational accuracy. Moreover, the proposed method outperformed the CBFM in terms of calculation precision.

4.3. Perfect Electrical Conductor Almond

Consider the bistatic RCS of a PEC almond-shaped target with a length of 504.748 mm. The incident frequency is 3 GHz. The almond target surface is discretized using RWG basis functions and meshed into 22048 triangular elements, yielding 33072 unknowns. Subsequently, the target is divided into 8 sub-blocks. After each sub-block is outward-extended by 0.15 wavelengths, a total of 48563 unknowns are obtained. With the SVD threshold set to 0.01, 1674 CBFs are extracted. Figure 9 compares horizontally polarized bistatic RCSs for this almond target calculated by different methods. Numerical results demonstrate that the proposed method achieves excellent computational accuracy.

Finally, Table 1 presents a comparative analysis of the computational time and RCS error between the CBFM-ACA and proposed methods for the three distinct models. The construction of basis functions involves both filling the impedance matrix and computing characteristic basis functions. Data analysis revealed that the proposed method achieved higher computational accuracy for three target types with only a slight increase in computational overhead. The solution accuracy was improved by 56.4%, 49.5%, and 42.6%, respectively, and the number of iterations was 23, 50, and 34.

5. CONCLUSION

This study proposes a novel scheme to improve the computational efficiency of the current coefficient reconstruction based on CBFM. Taking the ACA algorithm as the core acceleration technique, the proposed scheme introduces the ACA low-rank compression strategy at the Krylov-subspace iterative solution stage. The ACA algorithm is used to accurately exploit the low-rank property of impedance matrices, avoids] the heavy computational burden caused by the full assembly and storage of large-scale dense matrices in conventional algorithms, and significantly reduces the memory consumption and computational overhead. The construction accuracy of Krylov subspaces and iterative convergence criteria are optimized, which effectively improves the convergence behavior of the iterative solver, lowers residual computational cost, and further enhances the overall computational efficiency of iterative solutions. In addition, the numerical results of the proposed method are in good agreement with the reference results calculated by the commercial electromagnetic software FEKO, which fully validates the favorable reliability of the proposed method for analyzing complex electromagnetic structures.

ACKNOWLEDGEMENT

This work was supported in part by the Natural Science Research Project of Anhui Educational Committee under Grant No. 2025AHGXZK31006 and the Research Foundation of Jiangsu Engineering Research Center for Bionics Control Technology and Equipment under grant No. FSKZ202503, in part by the Anhui International Joint Research Center for Ancient Architecture Intelligence and Multi-Dimensional Modeling under No. GJZZX2025KF01.

REFERENCES

[1] Knott, E. F., J. F. Schaeffer, and M. T. Tulley, *Radar Cross Section*, 2nd ed., Artech House, Boston, USA, 1993.

[2] Harrington, R. F., *Field Computation by Moment Methods*, Macmillan, New York, 1968.

[3] Rao, S., D. Wilton, and A. Glisson, "Electromagnetic scattering by surfaces of arbitrary shape," *IEEE Transactions on Antennas and Propagation*, Vol. 30, No. 3, 409–418, 1982.

[4] Dugan, J., T. J. Smy, and S. Gupta, "Accelerated IE-GSTC solver for large-scale metasurface field scattering problems using fast multipole method (FMM)," *IEEE Transactions on Antennas and Propagation*, Vol. 70, No. 10, 9524–9533, 2022.

[5] Song, J., C.-C. Lu, and W. C. Chew, "Multilevel fast multipole algorithm for electromagnetic scattering by large complex objects," *IEEE Transactions on Antennas and Propagation*, Vol. 45, No. 10, 1488–1493, 1997.

[6] Tetzner, J. M. and S. B. Adrian, "On the adaptive cross approximation for the magnetic field integral equation," *IEEE Transactions on Antennas and Propagation*, Vol. 72, No. 12, 9366–9377, 2024.

[7] Zhao, K., M. N. Vouvakis, and J.-F. Lee, "The adaptive cross approximation algorithm for accelerated method of moments computations of EMC problems," *IEEE Transactions on Electromagnetic Compatibility*, Vol. 47, No. 4, 763–773, 2005.

[8] Peng, Z., X.-C. Wang, and J.-F. Lee, "Integral equation based domain decomposition method for solving electromagnetic wave scattering from non-penetrable objects," *IEEE Transactions on Antennas and Propagation*, Vol. 59, No. 9, 3328–3338, 2011.

[9] Prakash, V. V. S. and R. Mittra, "Characteristic basis function method: A new technique for efficient solution of method of moments matrix equations," *Microwave and Optical Technology Letters*, Vol. 36, No. 2, 95–100, 2003.

[10] Sun, Y. F., Y. Zhang, S. J. Xu, and X. Q. Chen, "EM scattering analysis of 2-D multiple conducting cylinders using characteristic basis function method," *Chinese Journal of Radio Science*, Vol. 21, No. 2, 229–232, 2006.

[11] Wang, Z.-G., W.-Y. Nie, and H. Lin, "Characteristic basis functions enhanced compressive sensing for solving the bistatic scattering problems of three-dimensional targets," *Microwave and Optical Technology Letters*, Vol. 62, No. 10, 3132–3138, 2020.

[12] Wang, P., Z.-G. Wang, Y.-F. Sun, and W.-Y. Nie, "Novel compressive sensing computing model used for analyzing electromagnetic scattering characteristics of three-dimensional electrically large objects," *Acta Physica Sinica*, Vol. 72, No. 3, 030202, 2023.

[13] Wang, Z., H. Yuan, Y. Sun, and W. Nie, "Fast solve of broadband electromagnetic scattering problems based on Krylov subspace basis functions combining with compressive sensing," *Microwave and Optical Technology Letters*, Vol. 67, No. 8, e70350, 2025.

[14] Wilton, D., S. Rao, A. Glisson, D. Schaubert, O. Al-Bundak, and C. Butler, "Potential integrals for uniform and linear source distributions on polygonal and polyhedral domains," *IEEE Transactions on Antennas and Propagation*, Vol. 32, No. 3, 276–281, 1984.

[15] Xu, Y., H. Yang, J. Lu, W. Yu, W. Yin, and D. Peng, "Improved synthetic basis functions method for nonperiodic scaling structures with arbitrary spatial attitudes," *IEEE Transactions on Antennas and Propagation*, Vol. 65, No. 9, 4728–4741, 2017.

[16] Wang, Z., H. Yuan, Y. Sun, W. Nie, and P. Wang, "Block-based Krylov subspace basis functions for solving bistatic scattering problems," *IEEE Antennas and Wireless Propagation Letters*, Vol. 22, No. 10, 2561–2565, 2023.

[17] Wang, Z., P. Wang, Y. Sun, and W. Nie, "Fast analysis of bistatic scattering problems for three-dimensional objects using compressive sensing and characteristic modes," *IEEE Antennas and Wireless Propagation Letters*, Vol. 21, No. 9, 1817–1821, 2022.

[18] Wang, Z., D. Dong, F. Guo, Y. Sun, W. Nie, and P. Wang, "Fast construction of measurement matrix and sensing matrix with dual adaptive cross approximation," *IEEE Antennas and Wireless Propagation Letters*, Vol. 24, No. 1, 13–17, 2025.

[19] Wang, Z., X. Tang, and Q. Wang, "Fast calculation of wide-angel RCS of objects using improved primary characteristic basis functions," *Journal of Electronics & Information Technology*, Vol. 40, No. 3, 573–578, 2018.

[20] Tanaka, T., K. Niino, N. Nishimura, M. Takikawa, and N. Yoneda, "A generation scheme of the characteristic basis functions by using block Krylov subspace algorithm," *Transactions of the Japan Society for Computational Engineering and Science*, Vol. 19, 99–102, 2019.

[21] Tanaka, T., K. Niino, N. Nishimura, and M. Takikawa, "Accuracy controllable characteristic basis function method by using Krylov subspace algorithm," *Transactions of the Japan Society for Computational Methods in Engineering*, Vol. 22, 11–19, 2022.

[22] Konno, K., Q. Chen, K. Sawaya, and T. Sezai, "Optimization of block size for CBFM in MoM," *IEEE Transactions on Antennas and Propagation*, Vol. 60, No. 10, 4719–4724, 2012.